Atmos. Chem. Phys., 25, 16817–16832, 2025 https://doi.org/10.5194/acp-25-16817-2025 © Author(s) 2025. This work is distributed under the Creative Commons Attribution 4.0 License.





Photochemical processing of dissolved organic matter in fog water: oxidation and functionalization pathways driving organic aerosol evolution

Wenging Jiang^{1,2}, Lijuan Li^{1,3}, Lu Yu^{1,2}, Hwajin Kim^{1,4}, Yele Sun^{1,5}, and Qi Zhang^{1,2}

¹Department of Environmental Toxicology, University of California, Davis, 1 Shields Ave., CA 95616, USA

²Agricultural and Environmental Chemistry Graduate Group, University of California,

Davis, 1 Shields Ave., CA 95616, USA

³Research Center for Atmospheric Environment, Chongqing Institute of Green and Intelligent Technology, Chinese Academy of Sciences, Chongqing 400714, China

⁴Department of Environmental Health Sciences, Seoul National University, Seoul 08826, South Korea ⁵State Key Laboratory of Atmospheric Environment and Extreme Meteorology, Institute of Atmospheric Physics, Chinese Academy of Sciences, Beijing 100029, China

Correspondence: Qi Zhang (dkwzhang@ucdavis.edu)

Received: 13 August 2025 – Discussion started: 28 August 2025 Revised: 11 October 2025 – Accepted: 8 November 2025 – Published: 26 November 2025

Abstract. Photochemical reactions of dissolved organic matter (DOM) in atmospheric waters can alter the composition and properties of organic aerosols (OA), with implications for climate and air quality. In this study, we investigated the aqueous-phase transformation of fog DOM under simulated sunlight using online aerosol mass spectrometry (AMS), offline Orbitrap mass spectrometry with electrospray ionization, UV-vis spectroscopy, and aerosol volatility measurements. Irradiation increased the mass concentration of DOM-derived OA (DOM_{OA}), defined as the low-volatility fraction of DOM that forms OA upon water evaporation. This increase was primarily driven by functionalization reactions that added oxygen- and nitrogen-containing groups, as indicated by a stable C mass, rising oxygen-to-carbon (O / C) and nitrogen-to-carbon (N / C) ratios, and enhanced signals of heteroatom-containing compounds over the course of irradiation. Despite evidence of fragmentation, spectral features associated with oligomerization, such as phenolic dimers, were also observed. To characterize chemical aging of fog DOM, we applied positive matrix factorization to the AMS spectra and identified three distinct factors representing progressive stages of aqueous-phase aging: initial DOM_{OA}, more oxidized intermediates, and highly oxidized products, characterized by progressively increasing O/C and N/C ratios. These findings demonstrate that sunlight-induced aqueous-phase oxidation and functionalization of fog DOM drive the formation and aging of secondary OA, altering its composition, volatility, and light-absorbing properties with potential atmospheric consequences.

1 Introduction

Dissolved organic matter (DOM) is a ubiquitous and chemically diverse component of cloud, fog, and rain droplets, where it plays a central role in the chemical and physical evolution of atmospheric aqueous systems. DOM originates from various sources, including the dissolution of soluble gases, uptake of hygroscopic particles, and multiphase oxi-

dation of hydrophobic compounds into water-soluble forms (Bianco et al., 2020; Collett et al., 2008; Herckes et al., 2013; Kim et al., 2019; Mazzoleni et al., 2010; Pratap et al., 2021; Schneider et al., 2017). As a result, its composition is highly complex (Bianco et al., 2018; Brege et al., 2018; Mazzoleni et al., 2010; Pailler et al., 2024; Sun et al., 2021; Zhao et al., 2013), encompassing both small polar molecules (e.g., organic acids, carbonyls, dicarbonyls, and organosul-

fates) (Altieri et al., 2009b; Boris et al., 2018; Herckes et al., 2002a; Liu et al., 2021; Pratt et al., 2013) and high molecular weight (HMW) species such as humic-like substances and secondary oligomers (Altieri et al., 2009b; Collett et al., 2008; Hawkins et al., 2016; Laskin et al., 2015; Renard et al., 2015; Sun et al., 2010). Primary particle tracers, such as *n*-alkanes, long-chain alkanoic acids, and polycyclic aromatic hydrocarbons (PAHs), have also been detected in fog and cloud droplets, though they typically represent only a minor fraction of dissolved carbon, even in heavily polluted areas (Collett et al., 2008; Ehrenhauser et al., 2012).

In addition to carbon-rich compounds, organic nitrogen (ON) and organic sulfur (OS) species are also prevalent in atmospheric waters. These include amines, N-containing heteroaromatics, nitrophenols, and nitrooxy-organosulfates (Altieri et al., 2009a; Desyaterik et al., 2013; Kim et al., 2019; Mattsson et al., 2025; Sun et al., 2024; Youn et al., 2015; Zhang et al., 2002; Zhang and Anastasio, 2003b), particularly in regions impacted by biomass burning and agricultural emissions (Collett et al., 2008; Li et al., 2023; Mattsson et al., 2025; Parworth et al., 2017; Zhang and Anastasio, 2001). ON and OS species can enter cloud and fog droplets via direct uptake of gaseous or particulate species, or they may form secondarily through aqueous-phase reactions involving precursors such as ammonia, amines, amino acids, and SO₂.

A wide range of VOCs (e.g., isoprene, monoterpenes, glyoxal, methylglyoxal, and phenols) contribute to DOM via gas-to-liquid partitioning followed by aqueous-phase reactions (Arciva et al., 2022; Ervens et al., 2008; Jiang et al., 2021; Tomaz et al., 2018; Wang et al., 2021; Yu et al., 2014; Zhang et al., 2024). These VOCs, along with pre-existing DOM, can undergo direct photolysis or react with a suite of oxidants, including hydroxyl radical (•OH), singlet oxygen (${}^{1}O_{2}^{*}$), hydrogen peroxide, peroxyl radicals, ozone (O_{3}), nitrate radical (•NO₃), sulfate radical (•SO₄⁻), and organic triplet excited states (3C*) (Bianco et al., 2020; Borduas-Dedekind et al., 2019; Hems et al., 2020; Herrmann et al., 2015; Jiang et al., 2023; Kaur et al., 2019; Smith et al., 2015; Tomaz et al., 2018; Zhang and Anastasio, 2003a). These reactions significantly alter the aqueous phase composition and, following droplet evaporation, influence the concentration, oxidation state (OS_C), and molecular makeup of the resulting organic aerosols (OA) (Farley et al., 2023; Hems et al., 2020; Kim et al., 2019; Lee et al., 2012; Renard et al., 2015; Schneider et al., 2017; Schurman et al., 2018). Consequently, aqueous-phase processing of DOM affects OA's light absorption and cloud activation properties, with broad implications for atmospheric chemistry and Earth's radiative budget (Borduas-Dedekind et al., 2019; Farley et al., 2023; Hems et al., 2020).

Despite growing recognition of the importance of aqueous-phase chemistry, significant knowledge gaps remain regarding the evolution of real-world DOM under ambient atmospheric conditions. These uncertainties limit our ability to

predict aerosol-cloud interactions, which represent one of the largest sources of uncertainty in climate models. While laboratory studies have yielded valuable mechanistic insights, they often rely on simplified model systems that don't capture the chemical complexity of ambient DOM. Other studies using real-world samples often employed non-atmospheric irradiation (e.g., 254 nm UV), reducing their relevance to atmospheric processes.

In this study, we examine the photochemical transformation of DOM in wintertime fog water collected in Fresno, California – a major urban center in the San Joaquin Valley (SJV), where fog plays a key role in winter aerosol pollution. The SJV has been the subject of extensive fog chemistry research (Collett et al., 2001; Collier et al., 2018; Ehrenhauser et al., 2012; Ge et al., 2012a; Herckes et al., 2015; Kim et al., 2019; Zhang and Anastasio, 2001), and Fresno fog water is known to contain a complex mixture of organic compounds spanning a wide range of chemical properties (Herckes et al., 2007; Kim et al., 2019; Mazzoleni et al., 2010; Zhang and Anastasio, 2001). Here, we define "DOM" as the total pool of dissolved organics, including water-soluble gases, and "DOMOA" as the low-volatility fraction that remains in the particle phase after fog water aerosolization and drying. We used a high-resolution time-of-flight aerosol mass spectrometer (HR-AMS) to track DOM_{OA} concentration and composition in real time during simulated sunlight illumination. Positive matrix factorization (PMF) was applied to the HR-AMS spectra to resolve distinct stages of aqueous-phase aging, complemented by molecular analysis using Orbitrap mass spectrometry with electrospray ionization (ESI-MS), UV-Vis spectroscopy, and thermodenuder measurements of aerosol volatility.

2 Experimental methods

2.1 Collection of fog water samples

The fog water samples were collected on 9 January 2010, in Fresno in the SJV of California, as detailed in Kim et al. (Kim et al., 2019). The sampling site was situated at a large agricultural field of California State University, Fresno (36°49'35.9" N, 119°44'42.7" W), in relatively close proximity to two major highways and a residential area (Ehrenhauser et al., 2012; Wang et al., 2013). Fog samples were collected using Caltech Active Strand Cloud Collectors (CASCC; $\sim 25.4 \,\mathrm{m}^3 \,\mathrm{min}^{-1}$ airflow) (Demoz et al., 1996) and a stainless steel extra-large CASCC collector (XL-CASS; $\sim 40 \, \mathrm{m}^3 \, \mathrm{min}^{-1}$ air flow) (Herckes et al., 2007). All samples were immediately filtered onsite using 0.22 µm glass fiber filters (Wang et al., 2013) and stored in the dark at -20 °C until use. The characteristics of the fog samples have been reported by Kim et al. (2019) and are summarized in Table S1 in the Supplement. Three consecutive fog samples with highly similar chemical composition were combined to yield approximately 110 mL of composite sample, the volume required for photooxidation experiments conducted in February 2015. Although multiyear storage can potentially affect certain labile compounds, these samples were also analyzed shortly after collection, and the results were reported previously (Kim et al., 2019). The HR-AMS spectrum of the unilluminated fog sample from this study is highly similar to the spectra reported by Kim et al. (2019), indicating that DOM_{OA} composition remained largely unchanged during storage. Additionally, the composition of the fog samples used in this study is also similar to other winter fog water samples from Fresno (Kim et al., 2019) and from Davis, CA, indicating their representativeness for winter fogs in California's Central Valley.

2.2 Photochemical oxidation

Aqueous oxidation was carried out using air-saturated fog water stirred in a Pyrex tube and exposed to simulated sunlight inside an RPR-200 Photoreactor System equipped with three types of bulbs emitting wavelengths of light centered at 300, 350 and 419 nm, respectively. Figure S1 in the Supplement shows the normalized photon fluxes inside the RPR-200 illumination system. In this setup, lamp emission below 315 nm is minimal, and the Pyrex tube further blocks wavelengths below 300 nm, effectively confining the actinic flux reaching the solution to the UVA and visible range. No additional optical filters were employed. Prior actinometry measurements of this RPR-200 illumination system indicate that its photochemical rate is ~ 7 times faster than that of winter solstice midday sunlight in Northern California (George et al., 2015). Accordingly, the $\sim 8 \, \mathrm{h}$ of illumination applied in our photochemical experiments corresponds to approximately 56 h of exposure to ambient sunlight. Under this condition, a variety of oxidants, such as hydroxyl radical (•OH), nitrate radical (•NO₃), triplet states of organic carbon (³C*), and singlet molecular oxygen (¹O₂*), can be produced during illumination and react with dissolved organics in the aqueous phase. ³C* can form when brown carbon chromophores in fog water absorb light and undergo intersystem crossing (McNeill and Canonica, 2016). Energy transfer between ³C* and dissolved O₂ yields ¹O₂* (Kaur and Anastasio, 2017; Ossola et al., 2021). H₂O₂ can be generated via energy/electron transfer of ³C* (Anastasio et al., 1997), which can subsequently undergo photolysis to produce •OH. Additionally, •OH can be generated from nitrate and nitrite photolysis in fog water (Brezonik and Fulkerson-Brekken, 1998). Previous studies have reported steady-state •OH concentration in fog water from Northern California (winter sunlight) in the range of $3.4 - 6.6 \times 10^{-16}$ M, and ${}^{1}O_{2}^{*}$ concentration of $1.1 - 6.1 \times 10^{-16}$ 10⁻¹³ M (Anastasio and McGregor, 2001). A Shimadzu LC-10AD high-performance liquid chromatography pump continuously drew solution at a flow rate of 0.2 mL min⁻¹ from the illuminated tube or a dark control tube wrapped entirely with aluminum foil. The effluent was atomized with nitrogen, fully dried using a diffusion dryer, and analyzed in realtime by HR-AMS. The non-refractory organics detected after this atomization-drying process are defined as DOM_{OA} , while compounds that completely volatilize during drying are not included. This nebulizer-dryer-AMS approach has been widely used in prior fog studies (Brege et al., 2018; Kim et al., 2019; Mattsson et al., 2025). The illuminated solution was continuously aerosolized and sampled until fully consumed, which took \sim 8 h. Additionally, aliquots of the illuminated fog water samples were collected over four consecutive time intervals (S1: 0–2 h, S2: 2–4 h, S3: 4–6 h, and S4: 6–8 h) and analyzed offline by electrospray ionization mass spectrometry (ESI-MS) and UV-vis spectroscopy.

2.3 HR-AMS measurement and data analysis

2.3.1 HR-AMS measurement and data analysis

Bulk chemical composition and elemental ratios of DOM_{OA} were analyzed using the HR-AMS, which employs 70 eV electron ionization (EI) mass spectrometry after aerosol evaporation at $\sim 600\,^{\circ}\text{C}$ (DeCarlo et al., 2006). The instrument was operated in both "V" and "W" ion optical modes, achieving mass resolutions of ~ 3000 and ~ 5000 , and capturing spectra up to m/z 500 and 300 amu, respectively.

HR-AMS data were processed using SQUIRREL v1.15 and PIKA v1.56 (http://cires.colorado.edu/jimenez-group/ ToFAMSResources/ToFSoftware/, last access: : 21 November 2025). W-mode data were used to obtain high-resolution mass spectra (HRMS) and derive elemental ratios, including oxygen-to-carbon (O / C), hydrogen-to-carbon (H / C), nitrogen-to-carbon (N/C), sulfur-to-carbon (S/C), and the organic mass-to-carbon ratio (OM / OC) (Aiken et al., 2008). With relative humidity at the HR-AMS inlet below 5 %, contributions from water vapor were considered negligible, and the organic H₂O⁺ signal was estimated by subtracting the sulfate-derived contribution from the total H₂O⁺ signal (Allan et al., 2004). To estimate the organic CO⁺ signal, we performed a separate, offline HR-AMS analysis of fog samples using argon as the atomization gas (Yu et al., 2014), which eliminates the interference from N_2 at m/z 28. The argon-atomized measurements showed that the CO⁺ signal was $\sim 31\%$ as intense as the CO_2^+ signal in DOM_{OA} mass spectra. This ratio ($CO^+ = 0.31 \times CO_2^+$) was then applied to the online N2-atomized HR-AMS data to improve the accuracy of DOM_{OA} O / C and OM / OC estimates.

2.3.2 Positive Matrix Factorization (PMF) analysis

PMF analysis was performed using the PMF2.exe algorithm in robust mode (Paatero and Tapper, 1994), via the PMF Evaluation Toolkit (PET) v2.06 (Ulbrich et al., 2009), http://cires.colorado.edu/jimenez-group/wiki/index.php/PMF-AMS_Analysis_Guide (last access: 21 November 2025). The input data included the ion-speciated HRMS matrix (containing 287 ions and 1001 time points)

and its corresponding error matrix, prepared following the refinement protocol outlined in Table 1 of Zhang et al. (2011).

To identify the optimal solution, PMF was run using factor numbers (p) from 1 to 5 and rotational parameters (fPeak) from -1.0 to 1.0 in 0.1 increment, as recommended by Zhang et al. (2011). After a thorough examination, the 3-factor solution with fPeak = -0.1 ($Q/Q_{exp} = 5.57$) was chosen. A summary of key diagnostic plots is presented in Fig. S2. This solution best captured both the total DOM_{OA} mass and its temporal evolution (Fig. S2f), with only minor variations across different fPeak values (Fig. S2c). For comparison, the 2-factor and 4-factor solutions are shown in Fig. S3, with diagnostics in Figs. S4–S5. The 2-factor solution underperformed during the initial irradiation phase, while the 4-factor solution split one interpretable component into two less meaningful factors. Overall, the 3-factor solution provided the most robust and interpretable description of DOM_{OA} evolution under simulated sunlight.

2.4 Determination of DOM_{OA} formation and decay rates for the three PMF factors

The formation and decay kinetics of DOM_{OA} associated with the three PMF factors were determined through curve fitting using Igor Pro 6.36 (Wavemetrics, Portland, OR, USA). The temporal evolution of each factor was modelled using exponential functions. The decay of Factor 1 was fitted using a pseudo first-order kinetic model:

$$[DOM_{OA-fac1}]_t = a + b \cdot \exp(-k_d t). \tag{1}$$

For Factor 2, both formation and decay processes were considered and modeled using a double exponential function:

$$[DOM_{OA-fac2}]_t = a + b \cdot \exp(-k_f t) + c \cdot \exp(-k_d t). \tag{2}$$

The formation rate of Factor 3 was modeled as a first-order process driven by the decay of Factor 2:

$$[DOM_{OA-fac3}]_t = a + b \cdot \exp(-k_f t). \tag{3}$$

Here, $[DOM_{OA-faci}]_t$ is the concentration of the ith DOM_{OA} factor at time t; a, b, and c are fitted coefficients; k_f and k_d represent apparent first-order formation and decay rate constants, respectively. These parameters were obtained by least-squares fitting the models to the experimental data.

2.5 ESI-MS analysis

Fog water samples collected over four irradiation time intervals, corresponding to distinct photochemical aging stages (Fig. S6), were analyzed using an LTQ Orbitrap mass spectrometer (Thermo Scientific, Inc.) equipped with an electrospray ionization (ESI) source operated in positive mode for molecular characterization. Winter fog DOM in Fresno is characterized by high N/C ratios and elevated concentrations of N-containing organics, such as amines, amino

acids and imidazoles (Kim et al., 2019), which are protonatable and exhibit strong sensitivity in positive-mode ESI. Given our interest in formation and transformation of organic nitrogen species, we analyzed the samples in positive mode. Mass spectrometry data were acquired using Xcalibur software, and individual MS peaks with signal-to-noise ratio (S/N) > 10 were extracted using the Decon2LS program. Subsequent processing and formula assignments were conducted with customized Microsoft Excel macros (Roach et al., 2011) based on Kendrick mass (KM) defect analysis with a KM base of CH₂, excluding ¹³C isotopes. Formula assignments were restricted by a mass accuracy threshold of < 5 ppm and the following elemental limits: $C \le 100$, $H \le 200$, $O \le 50$, $N \le 4$, $S \le 2$, and $Na \le 1$. Elemental ratios were confined to $0.0 \le H/C \le 3.0$ and $0.0 \le O/C \le 3.0$. The formulas of neutral species were subsequently determined by removing the adducting ions (e.g., H⁺ or Na⁺).

3 Results and discussion

3.1 Photochemical transformation of low-volatility organic species in fog water

Photochemical processing significantly altered the mass concentration and chemical composition of low-volatility organic solutes (DOM $_{OA}$) in fog water. As shown in Figs. 1d and S7, DOM $_{OA}$ increased from 25%–38% of total solute mass over \sim 8 h of simulated sunlight exposure – equivalent to roughly 56 h of winter solstice midday sunlight in Northern California based on actinometry measurements (George et al., 2015). In contrast, major inorganic species (i.e., nitrate, ammonia, sulfate, and chloride) remained largely unchanged, indicating net production of low-volatility organic compounds via aqueous-phase photochemistry.

Irradiation-induced changes in DOMOA composition are evident in the HR-AMS spectra (Figs. 1a-c). The O/C ratio increased from 0.60 prior to illumination (t_0) to 0.96 at t_{end} , and the fraction of CO_2^+ to total organic signal $(f_{CO_2^+})$ increased from 8.5 %-15.5 %, reflecting substantial oxidative aging processes. These changes are consistent with ambient wintertime observations in Fresno using real-time HR-AMS (Chen et al., 2018; Young et al., 2016). DOM_{OA} at t₀ resembled less-oxidized oxygenated OA (LO-OOA) and semi-volatile OOA (SV-OOA), while after irradiation it was more similar to more-oxidized OOA (MO-OOA) and lowvolatility OOA (LV-OOA) (Figs. 2d and S8). SV-OOA and LV-OOA are typically representative of relatively fresh and more-aged SOA, respectively (Ng et al., 2010). In addition, the nitrogen-to-carbon (N/C) ratio of DOM_{OA} increased from 0.045-0.054, indicating incorporation of nitrogen into the organic matrix, likely through reactions between DOM and N-containing nucleophiles such as ammonia, amino acids, and amines (Haan et al., 2009; Hawkins et al., 2016; Nozière et al., 2009; Shapiro et al., 2009). The AMS NO_2^+/NO^+ ratio decreased from 1.37–0.72 dur-

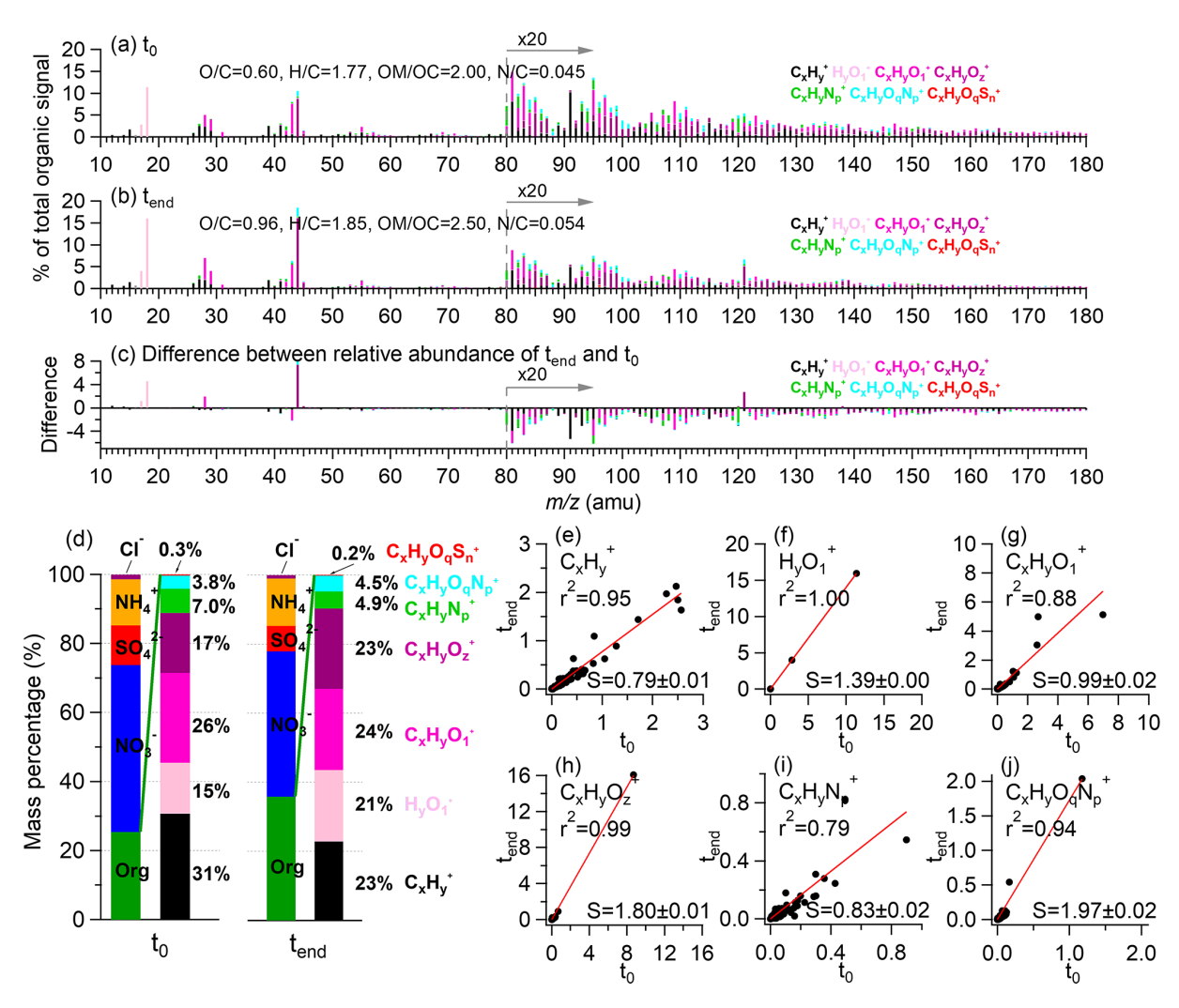


Figure 1. Overview of DOM_{OA} composition before (t_0) and after (t_{end}) eight hours of simulated sunlight illumination. (a–c) HR-AMS spectra of DOM_{OA} at t_0 and t_{end} , and the difference spectrum between them $(t_{end} \text{ minus } t_0)$, with peaks color-coded by ion categories: $C_xH_y^+$, $H_yO_1^+$, $C_xH_yO_1^+$, $C_xH_yO_z^+$, $C_xH_yO_p^+$, $C_xH_yO_qN_p^+$, $C_xH_yO_qS_n^+$ ($x \ge 1$; $y \ge 1$; z > 1; $p \ge 1$; $q \ge 1$; $n \ge 1$). Signals at $m/z \ge 80$ are multiplied by 20 for clarity. Elemental ratios are noted in the legend. (d) Mass fractions of major inorganic species and DOM_{OA} ion categories at t_0 and t_{end} (colors of ion categories match panels **a–c**). (**e–j**) Comparison of each ion category's signal contributions (% of total organic signal) at t_0 and t_{end} . Red lines show orthogonal distance regression (ODR) fits; slopes (S) and correlation coefficients (r^2) are provided in each panel.

ing illumination (Fig. S9), consistent with formation of low-volatility organic nitrates (Day et al., 2022; Farmer et al., 2010).

Figures 1e–j show scatter plots comparing the contributions of major HR-AMS ion families (i.e., $C_xH_y^+$, $H_yO_1^+$, $C_xH_yO_1^+$, $C_xH_yO_z^+$, $C_xH_yN_p^+$, and $C_xH_yO_qN_p^+$ ($x \ge 1$; $y \ge 1$; z > 1; $p \ge 1$; $q \ge 1$)) to the total organic signal at t_0 and $t_{\rm end}$. The corresponding comparisons of absolute ion signals are shown in Fig. S10. In most cases, orthogonal distance regression (ODR) slopes (S) significantly deviated from unity, highlighting systematic chemical evolution of DOM_{OA} during irradiation. The decreases of hydrocarbon-like ions ($C_xH_y^+$, S = 0.79; Fig. 1e) suggest fragmentation of carbon

backbones via photooxidation. In HR-AMS, organic-derived $H_yO_1^+$ ions are generated during vaporization and ionization of oxygenated organics such as carboxylic acids and alcohols (Canagaratna et al., 2015). In Fig. 1f, $H_yO_1^+$ ions showed a slope of 1.39, suggesting formation of oxygenated organics. The overall fractional contribution of the lightly oxygenated ion family $(C_xH_yO_1^+)$ remained unchanged during illumination (S=0.99; Fig. 1g). However, several individual ions departed significantly from the 1:1 line, indicating compositional change within the family. In contrast, the relative abundance of more oxygenated ions $(C_xH_yO_z^+; \text{ Fig. 1h})$ increased sharply (S=1.80), and their tightly correlated spectral patterns at t_0 and t_{end} $(r^2=0.99)$ suggest formation

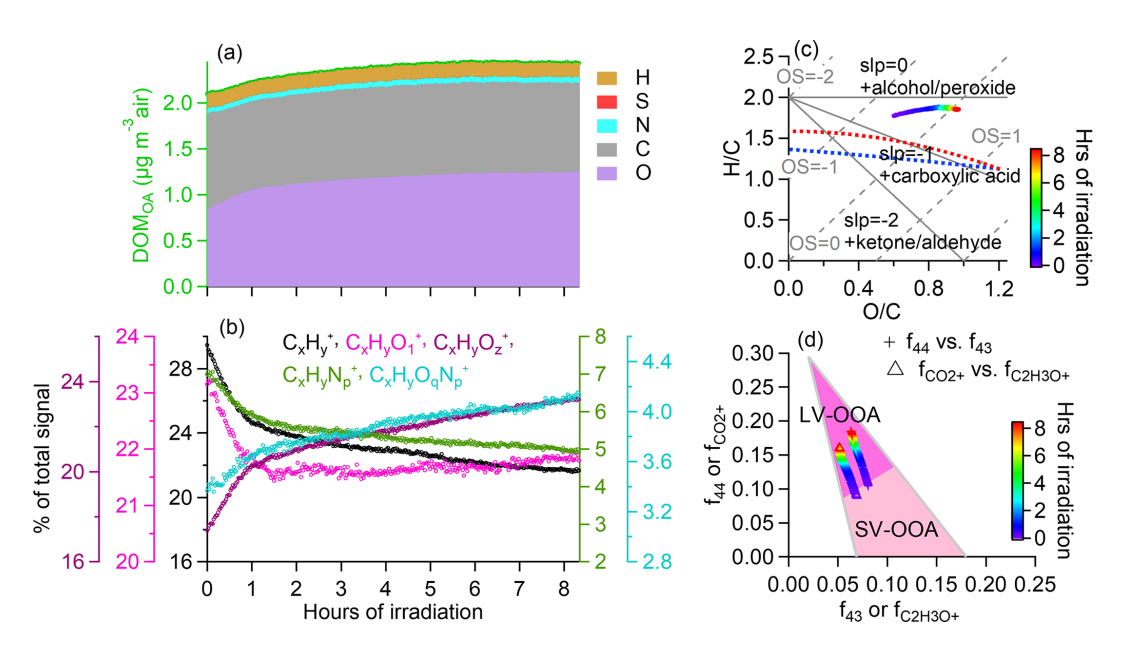


Figure 2. Time evolution of DOM_{OA} composition during simulated sunlight illumination. (a) DOMOA concentration and stacked mass contributions from O, C, N, S and H atoms. The mass concentrations represent ambient air concentrations, calculated by normalizing the liquid-phase concentrations to the sampled air volumes. (b) Fractional contributions of major ion categories to the total DOM_{OA} signals in HR-AMS spectra: $C_xH_y^+$, $C_xH_yO_1^+$, $C_xH_yO_z^+$, $C_xH_yN_p^+$, and $C_xH_yO_qN_p^+$ ($x \ge 1$; $y \ge 1$; z > 1; $p \ge 1$; $q \ge 1$). (c) Evolution profiles of DOM_{OA} in Van Krevelen space based on AMS measurements. (d) Evolution of f_{44} (fraction of m/z 44 in the AMS organic spectrum), f_{43} (fraction of m/z 43), $f_{CO_2^+}$ (fraction of CO_2^+ ion) and $f_{C_2H_3O^+}$ (fraction of $C_2H_3O^+$ ion). In this study, CO_2^+ dominates m/z 44 (83 %–88 %), with minor contributions from $C_2H_6N^+$ and CH_2NO^+ . $C_2H_3O^+$ dominates m/z 43, with $C_3H_7^+$, $C_2H_5N^+$, and $CHNO^+$ contributing the remainder. The shaded triangle area denotes the region where most ambient oxygenated organic aerosol (OOA) falls into, with the upper-right corner characteristic of low-volatility OOA (LV-OOA) and the lower-right corner of semi-volatile OOA (SV-OOA) (Ng et al., 2010, 2011).

of highly oxidized species with structural similarity to preexisting compounds. The dominance of CO_2^+ and CHO_2^+ within this family suggests carboxylation as a major pathway. In parallel, reduced organic nitrogen ions $(C_xH_yN_p^+;$ Fig. 1i) decreased in relative abundance (S=0.83), while oxidized organic nitrogen ions $(C_xH_yO_qN_p^+;$ Fig. 1j) increased (S=1.97). Consequently, the $C_xH_yN_p^+/C_xH_yO_qN_p^+$ ratio decreased from 2.1–1.2 (Fig. S11), consistent with oxidative transformation and functionalization of ON species during aqueous-phase processing.

Figure 2 illustrates the temporal evolution of DOM_{OA} during irradiation. Its mass concentration increased steadily (Fig. 2a), accompanied by rising O/C and N/C ratios, indicating continuous photochemical transformation. Despite these changes, the total carbon concentration remained nearly constant over 8 h of irradiation (RSD = 1.3%, Fig. 2a), suggesting minimal carbon loss to the gas phase. While previous studies have reported that $\sim 10\%$ of dissolved organic carbon in fog can be small volatiles such as acetate, formate, and formaldehyde (Herckes et al., 2002b), such VOCs were not detected in our samples (Kim et al., 2019). Although some volatilization during storage is possible, samples were stored in sealed containers at -20°C in the dark, minimizing reaction losses. As shown in Fig. 2a,

the observed DOM_{OA} mass increase was primarily driven by oxygen incorporation, with nitrogen addition playing a lesser role.

Figures 2b and S12 provide further insights into the photochemical evolution of DOM_{OA} through temporal trends and correlation analysis of five major HR-AMS ion categories. Signals from less oxygenated species $(C_xH_y^+, C_xH_yO_1^+)$ and $C_xH_yN_p^+$ decreased in their contribution to the total organic signal with irradiation, while more oxidized and nitrogenfunctionalized categories $(C_xH_yO_z^+)$ and $C_xH_yO_qN_p^+$ increased, indicating progressive oxidation and nitrogen incorporation. The decline in $C_xH_y^+$ reflects the breakdown of aliphatic and aromatic precursors, while the rise in $C_xH_yO_z^+$ and $C_xH_yO_qN_p^+$ is consistent with enhanced oxygenation and functionalization.

Strong negative correlations between $C_xH_y^+$ and both $C_xH_yO_z^+$ and $C_xH_yO_qN_p^+$ support the conversion of less oxidized compounds into highly oxygenated species. Additionally, positive correlations among O- and N-containing ions suggest shared aqueous-phase formation pathways, potentially involving reactions with nitrogenous species such as ammonium, amines, or organic nitrates. Collectively, these results highlight the extensive molecular transformation of DOM_{OA} during photochemical aging, involving both func-

tionalization and fragmentation, with a net buildup of highly functionalized organics. The evolving HR-AMS ion signatures are consistent with the aqueous-phase formation of SOA-like material under atmospheric conditions.

Insights into photochemical aging pathways of fog DOM

Photochemical aging of fog DOM involves both fragmentation of high-molecular-weight compounds and formation of highly functionalized, O- and N-containing species, as revealed by complementary ESI-MS and HR-AMS analyses.

Molecular-level insights from positive-mode ESI-MS corroborated the HR-AMS findings. As shown in Fig. S13, the relative abundance of CHN compounds decreased from 7.3 %–3.7 % over 8 h of irradiation, while the CHONS compounds increased from 27.4 %-39.5 %. The total CHON fraction remained relatively stable (38.9 %-40 %), but individual compounds, such as C₉H₁₇NO₈, increased markedly (Fig. 3a), suggesting oxidative conversion of CHN species (e.g., amines, imines, and heterocyclics) into more oxidized forms. The CHN species that decreased during irradiation were primarily C7-C16 compounds (Fig. 3c), whereas the CHON increases were mainly driven by C₉ species and the CHONS increases were associated with smaller molecules (e.g., C₂, C₃, C₄, and C₁₁) (Fig. 3f and h). These shifts in carbon number indicate fragmentation pathways that produce smaller O-, N-, and S-containing products.

Fragmentation was also evident in HR-AMS data, with high-mass ion signals declining after irradiation. As shown in Fig. 4, the unit mass resolution (UMR) spectra of DOM_{OA} in the m/z 180–450 range showed widespread signal reductions consistent with the breakdown of HMW species known to present in fog water (Ehrenhauser et al., 2012; Herckes et al., 2002b; Mazzoleni et al., 2010). However, a set of peaks (e.g., m/z 214, 230, 258, 275, 334, and 350) increased in intensity, with some spaced by 16 amu – indicative of progressive oxygen addition through reactions such as hydroxylation, peroxide formation, or radical-mediated reactions. This interpretation is also supported by the evolution of H / C and O/C ratios in Van Krevelen space (Fig. 2c), which follows a near-zero slope, consistent with net oxygen incorporation. Additionally, the fractional contribution of CHO₂⁺ to the total organic signal gradually increased from 0.63 %-0.93 % during irradiation (Fig. S14), suggesting that carboxylation played an important role in the formation of functionalized products. High-resolution peak fitting of these increased ions indicates that they either contain nitrogen or consist solely of C, H and O (Fig. S15). These results imply that photochemical aging of fog DOM involves both loss of HMW compounds and formation of new functionalized products.

Notably, the m/z 306 signal, a known tracer ion for syringol dimer formation (Sun et al., 2010; Yu et al., 2014), was enhanced following irradiation. Syringol, a methoxyphenol commonly emitted during biomass burning, is likely present

in the fog water due to winter residential wood burning in the region (Chen et al., 2018; Ge et al., 2012b; Young et al., 2016). The enhancement of m/z 306 provides direct evidence of aqueous-phase oligomerization of biomass burning-derived phenolic precursors, consistent with prior laboratory (Huang et al., 2018; Jiang et al., 2021, 2023; Yu et al., 2016) and field studies showing photooxidation of phenolics leads to hydroxylation, ether formation, and oligomerization (Gilardoni et al., 2016).

Together, these findings highlight the dual role of aqueousphase photochemistry: simultaneous fragmentation of existing DOM and generation of new, more oxygenated species with enhanced functionality. The concurrent increases in oxidation and nitrogen incorporation are consistent with aqueous-phase aging pathways that produce SOA-like material enriched in O- and N-functional groups.

3.3 Characterizing aqueous phase photoaging of DOM_OA via PMF

We applied PMF to the HR-AMS spectra to further resolve the progressive aqueous-phase aging of DOM_{OA} during simulated sunlight irradiation. This analysis allows us to deconvolve overlapping transformation processes and link them to chemical composition and reactivity. Three distinct factors were identified (Fig. 5), each corresponding to a different stage of photochemical processing. Factor 1 represented the initial DOM_{OA}, characterized by O/C = 0.66, H/C = 1.82, $OS_C = -0.5$, and N/C of 0.036. Its mass spectrum closely matched that of the bulk DOM_{OA} at t_0 . This factor decayed rapidly, with a first-order loss rate constant of $k_d = 2.0 \,\mathrm{h^{-1}}$. Factor 2 emerged shortly after the start of illumination and peaked around 1.5 h, increasing with a formation rate constant of $k_f = 2.6 \,\mathrm{h}^{-1}$ before gradually declining at $k_d = 0.016 h^{-1}$. This intermediate factor exhibited increased oxidation (O/C = 0.96) and a slightly higher N/C (=0.038) compared to Factor 1, indicating the incorporation of oxygenated functional groups into DOM. The transient nature and intermediate oxidation level of Factor 2 imply that it represented a key transformation stage, where precursor molecules were actively undergoing aqueous-phase reactions, likely including hydroxylation, carbonyl formation, and nitrogenation (Hawkins et al., 2016; Herrmann et al., 2015; Renard et al., 2015), on their way to forming more stable, low-volatility products.

Factor 3, the most oxidized component with the highest O / C (1.12) and N / C (0.040) ratios, accumulated gradually throughout the irradiation period, with an estimated formation rate constant of $k_{\rm f} = 0.13\,{\rm h}^{-1}$. This factor was enriched in highly oxygenated fragments (e.g., $C_x H_y O_z^+$), including ions such as CO_2^+ and CHO_2^+ , which are markers for carboxylic acids and other highly oxidized organic compounds. The elevated N / C ratio of Factor 3 (0.040 vs. 0.036 for Factor 1) indicates nitrogen incorporation into DOM_{OA} during photochemical aging. This conclusion is supported by multi-

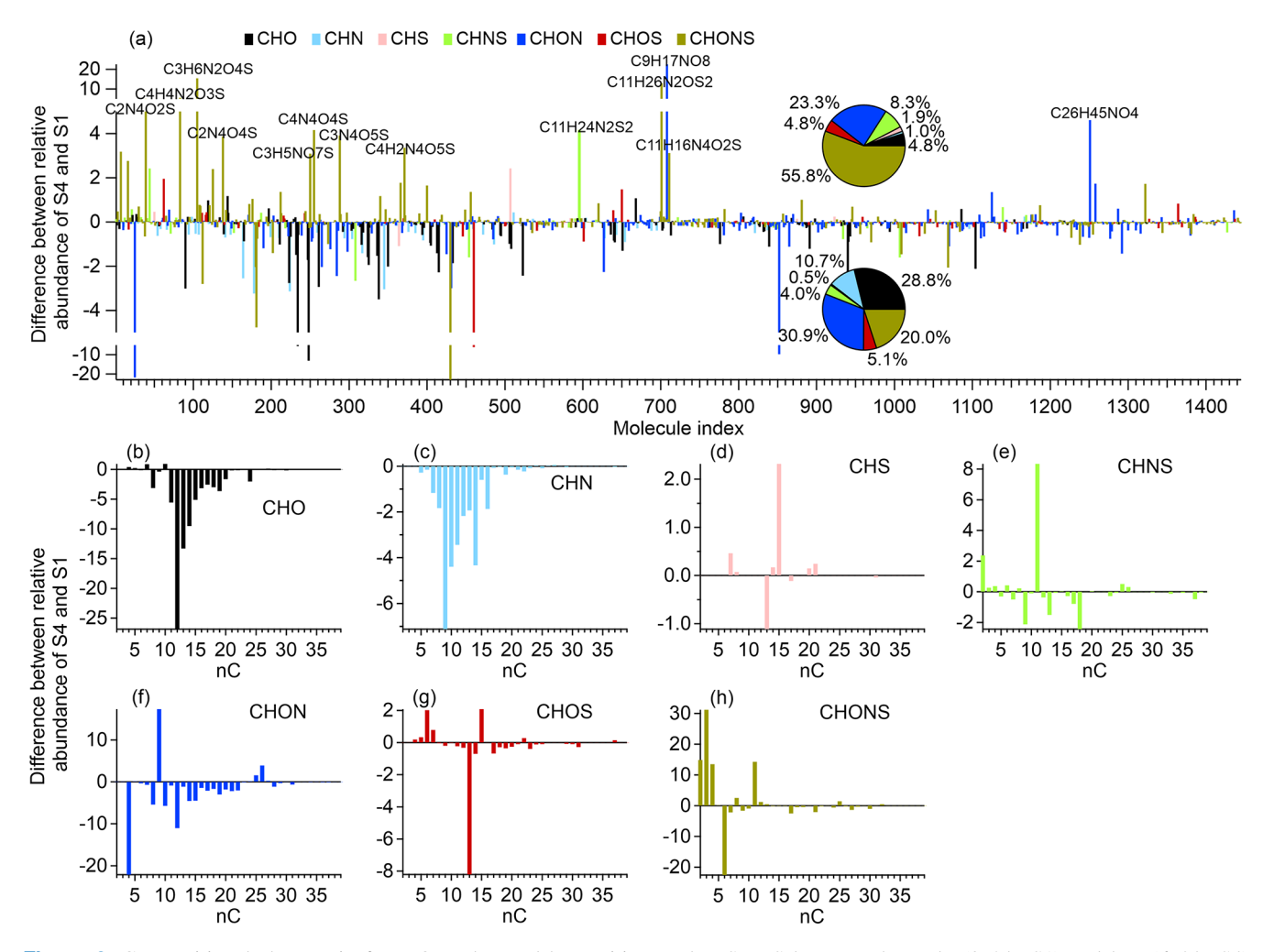


Figure 3. Compositional changes in fog DOM observed by positive-mode ESI-MS between the early (0–2 h, S1) and late (6–8 h, S4) irradiation periods. (a) Difference in relative abundance of all detected molecular formulas between S1 and S4; (b–h) Histograms showing changes in relative abundance of compounds grouped by carbon number for each molecular class: CHO, CHN, CHS, CHNS, CHON, CHOS, and CHONS.

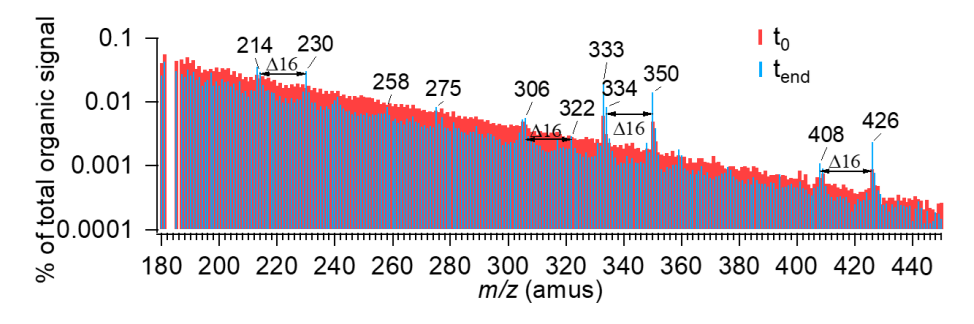


Figure 4. Comparison of unit mass resolution (UMR) spectra of DOM_{OA} in fog water before (t_0 , blue) and after (t_{end} , red) simulated sunlight illumination, over the m/z range 180–450 amu.

ple observations: over illumination, the low-volatility nitrogen mass increased from 0.055 to 0.062 $\mu g\,m^{-3}$; the N/C ratio of DOM_{OA} increased from 0.045–0.054; and the AMS NO $_2^+/NO^+$ ratio decreased from 1.37–0.72, a shift commonly interpreted as increased contribution of organic ni-

trates (Day et al., 2022; Farmer et al., 2010). The sustained increase in Factor 3 suggests that aqueous-phase photochemistry leads to the formation of a highly functionalized, low-volatility organic fraction that may be a significant contributor to SOA-like material in ambient fog or cloud water.

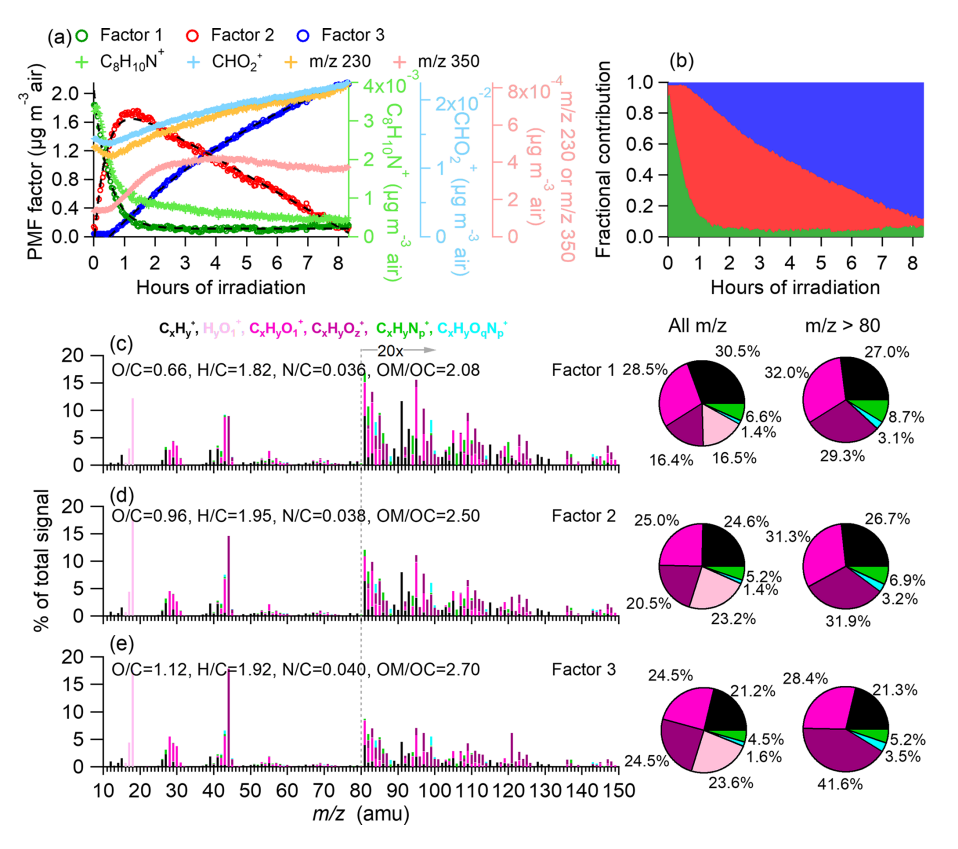


Figure 5. (a) Time series of the three-factor PMF solutions as well as tracer ions (e.g., $C_8H_{10}N^+$, CHO_2^+ , m/z 230, and m/z 350) representative of the three PMF factors. Factor 1 is fitted with a three-parameter single exponential function: $DOM_{OA-Fac1} = 0.11 + 1.9e^{-2.0t}$. Factor 2 is fitted with a five-parameter double exponential function: $DOM_{OA-Fac2} = 15.6 - 2.1e^{-2.6t} - 13.6e^{0.016t}$. Factor 3 is fitted with a three-parameter single exponential function: $DOM_{OA-Fac3} = 3.3 - 3.6e^{-0.13t}$. (b) Fractional contributions of the three PMF factors over time. (c-e) HR-AMS spectra of Factor 1, Factor 2, and Factor 3, respectively, with ion signals color-coded by six categories: $C_xH_y^+$, $H_yO_1^+$, $C_xH_yO_1^+$, $C_xH_yO_2^+$, $C_xH_yO_p^+$, and $C_xH_yO_qN_p^+$. Ion signals at $m/z \ge 80$ are enhanced by a factor of 20 for clarity. Calculated atomic ratios are shown in the legends. The pie charts show the relative contributions of different ion categories to each factor.

3.4 Photoinduced changes in light absorption and volatility of fog DOM

The optical properties of DOM in atmospheric waters have received increasing attention due to their contribution to brown carbon and their influence on Earth's radiative balance through solar absorption (Shapiro et al., 2009). To examine how fog water DOM evolves under photochemical processing, we measured its UV-visible absorbance at defined time intervals throughout the experiment. As shown in Fig. 6a, the initial fog water DOM exhibited strong absorbance in both the UV and visible regions, particularly between 300 and 500 nm relevant to tropospheric solar radiation. This absorption is attributed to conjugated chromophores, including HMW aromatic and polymeric compounds.

Despite substantial chemical transformation of the DOM (e.g., increased oxidation, nitrogen incorporation, molecular fragmentation, and polymerization), the overall UV-vis spectrum revealed only modest changes over the 8 h irradiation period. Differential absorbance spectra (relative to the

initial sample, S1; Fig. 6b) revealed a slight increase in the 280–350 nm range, suggesting the formation of new lightabsorbing chromophores during photochemical aging. These results indicate that aqueous-phase oxidation can sustain, and in some cases regenerate, the light-absorbing functionality of fog water DOM. This is consistent with AMS and ESI-MS observations of CHON species formation, which likely include chromophores such as nitroaromatics and imidazoles. Although photobleaching of brown carbon chromophores is frequently assumed and has been widely observed during atmospheric aging (Hems and Abbatt, 2018; Laskin et al., 2015; Leresche et al., 2021), both laboratory and field studies have shown that aging can also enhance light absorption through the formation of new chromophores (Bianco et al., 2020; Hems et al., 2021; Laskin et al., 2025; Wu et al., 2024). Consistent with these observations, our experiments indicate that brown carbon-like optical properties can persist or even intensify during aqueous-phase processing. In particular, we observed evidence of oligomer formation, which likely contributes to the generation of new light-absorbing

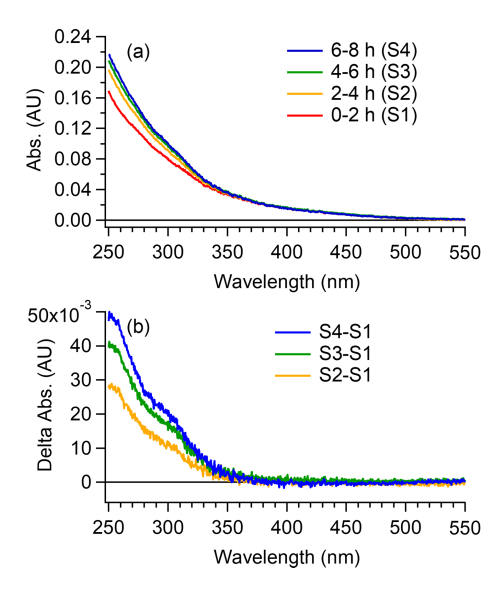


Figure 6. Evolution of UV-visible absorption of fog water sample during simulated sunlight exposure. (a) UV-visible absorbance spectra of fog water samples collected at successive illumination intervals: S1 (0–2 h), S2 (2–4 h), S3 (4–6 h) and S4 (6–8 h). (b) Differential absorbance spectra of samples S2–S4 relative to the initial sample S1.

species. These processes have important implications for the radiative forcing potential of aged OA.

To measure volatilities of fog-derived aerosols, we analyzed samples using HR-AMS downstream of a digitally controlled thermodenuder (TD, Fierz et al., 2007), which included a bypass line and a heated line ending in an activated carbon cloth section. The TD cycled through seven set temperatures (25, 40, 65, 85, 100, 150, and 200 °C) hourly, with an automated three-way valve switching between bypass and heated modes every 5 min. Comparing AMS signals between these modes allowed us to assess the volatility profiles of fog water-derived aerosols. Figure 7 shows the mass fraction remaining (MFR) of organic materials (DOM_{OA}), sulfate, and nitrate as a function of thermodenuder temperature over different irradiation periods. While sulfate (Fig. 7b) and nitrate (Fig. 7c) displayed consistent volatility profiles throughout the experiment, DOM_{OA} (Fig. 7a) exhibited a clear evolution over time. Specifically, the MFR curves became progressively less steep with increased irradiation, indicating the net formation of less volatile organic species. This trend is consistent with our chemical analyses results, which show increased formation of multifunctional products and oligomers. The accumulation of highly functionalized, lowvolatility compounds through aqueous-phase photochemical reactions may significantly impact the atmospheric lifetime and climate-relevant properties of OA.

4 Conclusions and atmospheric implications

This study examined the photochemical transformation of low-volatility DOM in fog water under simulated sunlight, equivalent to $\sim 56\,\mathrm{h}$ of wintertime tropospheric aging. The mass concentration of fog-derived DOM_OA increased steadily during illumination, largely due to functionalization reactions that incorporated O- and N-containing groups. Despite evidence of molecular fragmentation, total carbon mass remained largely stable, suggesting limited formation of volatile organics during aqueous-phase aging.

Both HR-AMS and positive-mode ESIMS revealed increases in N-containing species following irradiation, along with the photooxidative transformation of CHN compounds into more oxygenated CHON and CHONS species. PMF analysis of the HR-AMS spectra resolved three distinct aging stages: unprocessed DOM_{OA} (Factor 1; O/C = 0.66, H/C = 1.82, N/C = 0.036), more oxidized intermediates (Factor 2; O/C = 0.96, H/C = 1.95, N/C = 0.038), and highly oxidized products (Factor 3; O/C = 1.12, H/C = 1.92, N/C =0.040), with increasing O / C and N / C ratios across the factors. The accumulation of Factor 3 highlights fog processing as a source of O- and N-rich OA, potentially influencing aerosol hygroscopicity, light absorption, and toxicity. Supporting UV-vis and thermodenuder measurements confirmed that DOM_{OA} became increasingly more light-absorbing and less volatile with irradiation, consistent with the formation of highly functionalized, low-volatility species. Our findings are consistent with recent field observations in the Po Valley, Italy (Mattsson et al., 2025), which reported ON enhancement in fog water and fog residuals and attributed it to aqueous-phase formation of imidazoles. Although the Po Valley site is rural and our Fresno site is urban, both represent winter basin environments characterized by abundant liquid water and elevated nitrogen levels that favor aqueous processing and promote ON formation. The agreement between the Po Valley field observations and our laboratory aging experiments of Fresno fog DOM indicates that aqueous ON chemistry in fog is a broadly relevant pathway that may operate in diverse regions, with its magnitude influenced by local meteorology and emission sources. Overall, these results demonstrate that fog droplets act as chemically active microreactors, transforming dissolved organic matter into more oxidized, more light-absorbing and less volatile OA species during photochemical aging, beyond simply serving as scavengers of atmospheric pollutants (Collett et al., 2001, 2008; Kuang et al., 2020). Extensive laboratory and field studies have shown that oligomerization, acid formation, and imidazole formation proceed efficiently in the aqueous phase, producing aqSOA and brown carbon chromophores that can modify aerosol composition, light absorption, and hygroscopicity (Faust et al., 2017; Herrmann et al., 2015; Kuang et al., 2020; McNeill, 2015). Our results are consistent with prior findings and provide additional evidence for the influence of fog-driven aqueous processing on OA composi-

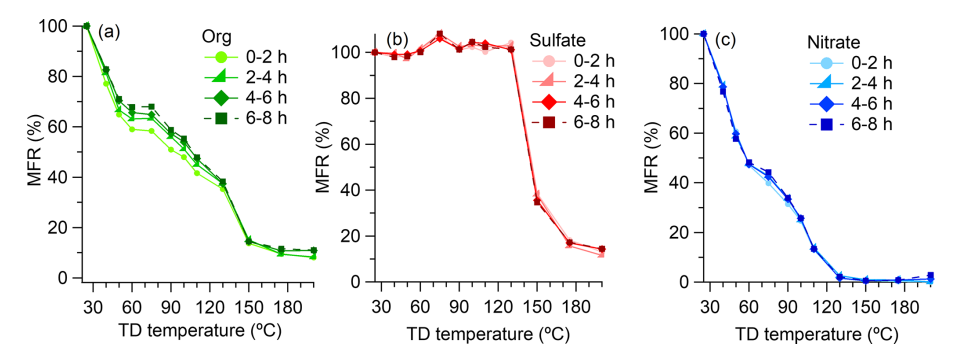


Figure 7. Mass fraction remaining (MFR, %) of **(a)** organics, **(b)** sulfate, and **(c)** nitrate in fog water-derived aerosols as a function of thermodenuder temperature. Each panel displays MFR trends across four irradiation periods (0–2, 2–4, 4–6, and 6–8 h of simulated sunlight illumination).

tion, ON speciation, volatility and light absorption. Given the frequent occurrence of winter fog and biomass burning in regions like California's San Joaquin Valley, fog-driven aqueous-phase processing likely plays a key role in regulating the atmospheric fate and climate-relevant properties of organic carbon and nitrogen. Although this study focuses on fog chemistry, similar processes are likely to occur in cloud water, with important implications for aerosol-cloud interactions and the oxidative evolution of atmospheric organic matter.

Code availability. All data and code used in the study are available from the corresponding author upon request.

Supplement. The supplement related to this article is available online at https://doi.org/10.5194/acp-25-16817-2025-supplement.

Author contributions. LY, HK and YS collected fog samples and conducted experiments. WJ, LL, and LY analyzed the data. WJ, LY, and QZ wrote the manuscripts with input from all authors. QZ guided the research, managed the project, and defined the overarching strategy.

Competing interests. The contact author has declared that none of the authors has any competing interests.

Disclaimer. Publisher's note: Copernicus Publications remains neutral with regard to jurisdictional claims made in the text, published maps, institutional affiliations, or any other geographical representation in this paper. While Copernicus Publications makes every effort to include appropriate place names, the final responsibility lies with the authors. Views expressed in the text are those of the authors and do not necessarily reflect the views of the publisher.

Acknowledgements. This research was supported by the US Department of Energy (DOE) Office of Science, Office of Biological and Environmental Research (BER), through the Atmospheric System Research (ASR) program (DE-SC00221400), the US National Institute of Environmental Health Sciences Core Center (grant P30 ES023513), and the California Agricultural Experiment Station (Projects CA-D*-ETX-2102-H). Additional support for Wenqing Jiang and Lu Yu was provided by the Jastro-Shields Graduate Research Award and the Donald G. Crosby Graduate Fellowship at UC Davis. We thank Pierre Herckes (ASU) for assisting with the Fresno fog sample collection.

Financial support. This research has been supported by the US Department of Energy (grant-no. DE-SC00221400), the Division of Agriculture and Natural Resources, University of California (grant-no. CA-D*-ETX-2102-H), and the National Institute of Environmental Health Sciences (grant-no. P30 ES023513).

Review statement. This paper was edited by Theodora Nah and reviewed by three anonymous referees.

References

- Aiken, A. C., DeCarlo, P. F., Kroll, J. H., Worsnop, D. R., Huffman, J. A., Docherty, K. S., Ulbrich, I. M., Mohr, C., Kimmel, J. R., Sueper, D., Sun, Y., Zhang, Q., Trimborn, A., Northway, M., Ziemann, P. J., Canagaratna, M. R., Onasch, T. B., Alfarra, M. R., Prevot, A. S. H., Dommen, J., Duplissy, J., Metzger, A., Baltensperger, U., and Jimenez, J. L.: O/C and OM/OC Ratios of Primary, Secondary, and Ambient Organic Aerosols with High-Resolution Time-of-Flight Aerosol Mass Spectrometry, Environ. Sci. Technol., 42, 4478–4485, https://doi.org/10.1021/es703009q, 2008.
- Allan, J. D., Bower, K. N., Coe, H., Boudries, H., Jayne, J. T., Canagaratna, M. R., Millet, D. B., Goldstein, A. H., Quinn, P. K., Weber, R. J., and Worsnop, D. R.: Submicron aerosol composition at Trinidad Head, California, during ITCT 2K2: Its relationship with gas phase volatile organic carbon and assessment of instrument performance, J. Geophys. Res.-Atmos., 109, https://doi.org/10.1029/2003JD004208, 2004.
- Altieri, K. E., Turpin, B. J., and Seitzinger, S. P.: Composition of Dissolved Organic Nitrogen in Continental Precipitation Investigated by Ultra-High Resolution FT-ICR Mass Spectrometry, Environ. Sci. Technol., 43, 6950–6955, https://doi.org/10.1021/es9007849, 2009a.
- Altieri, K. E., Turpin, B. J., and Seitzinger, S. P.: Oligomers, organosulfates, and nitrooxy organosulfates in rainwater identified by ultra-high resolution electrospray ionization FT-ICR mass spectrometry, Atmos. Chem. Phys., 9, 2533–2542, https://doi.org/10.5194/acp-9-2533-2009, 2009b.
- Anastasio, C. and McGregor, K. G.: Chemistry of fog waters in California's Central Valley: 1. In situ photoformation of hydroxyl radical and singlet molecular oxygen, Atmos. Environ., 35, 1079–1089, https://doi.org/10.1016/S1352-2310(00)00281-8, 2001.
- Anastasio, C., Faust, B. C., and Rao, C. J.: Aromatic Carbonyl Compounds as Aqueous-Phase Photochemical Sources of Hydrogen Peroxide in Acidic Sulfate Aerosols, Fogs, and Clouds. 1. Non-Phenolic Methoxybenzaldehydes and Methoxyacetophenones with Reductants (Phenols), Environ. Sci. Technol., 31, 218–232, https://doi.org/10.1021/es960359g, 1997.
- Arciva, S., Niedek, C., Mavis, C., Yoon, M., Sanchez, M. E., Zhang, Q., and Anastasio, C.: Aqueous •OH Oxidation of Highly Substituted Phenols as a Source of Secondary Organic Aerosol, Environ. Sci. Technol., 56, 9959–9967, https://doi.org/10.1021/acs.est.2c02225, 2022.
- Bianco, A., Deguillaume, L., Vaïtilingom, M., Nicol, E., Baray, J.-L., Chaumerliac, N., and Bridoux, M.: Molecular Characterization of Cloud Water Samples Collected at the Puy de Dôme (France) by Fourier Transform Ion Cyclotron Resonance Mass Spectrometry, Environ. Sci. Technol., 52, 10275–10285, https://doi.org/10.1021/acs.est.8b01964, 2018.
- Bianco, A., Passananti, M., Brigante, M., and Mailhot, G.: Photochemistry of the Cloud Aqueous Phase: A Review, Molecules, 25, 423, https://doi.org/10.3390/molecules25020423, 2020.
- Borduas-Dedekind, N., Ossola, R., David, R. O., Boynton, L. S., Weichlinger, V., Kanji, Z. A., and McNeill, K.: Photomineralization mechanism changes the ability of dissolved organic matter to activate cloud droplets and to nucleate ice crystals, Atmos.

- Chem. Phys., 19, 12397–12412, https://doi.org/10.5194/acp-19-12397-2019, 2019.
- Boris, A. J., Napolitano, D. C., Herckes, P., Clements, A. L. and Collett Jr, J. L.: Fogs and Air Quality on the Southern California Coast, Aerosol Air Qual. Res., 18, 224–239, https://doi.org/10.4209/aaqr.2016.11.0522, 2018.
- Brege, M., Paglione, M., Gilardoni, S., Decesari, S., Facchini, M. C., and Mazzoleni, L. R.: Molecular insights on aging and aqueous-phase processing from ambient biomass burning emissions-influenced Po Valley fog and aerosol, Atmos. Chem. Phys., 18, 13197–13214, https://doi.org/10.5194/acp-18-13197-2018, 2018.
- Brezonik, P. L. and Fulkerson-Brekken, J.: Nitrate-Induced Photolysis in Natural Waters: Controls on Concentrations of Hydroxyl Radical Photo-Intermediates by Natural Scavenging Agents, Environ. Sci. Technol., 32, 3004–3010, https://doi.org/10.1021/es9802908, 1998.
- Canagaratna, M. R., Jimenez, J. L., Kroll, J. H., Chen, Q., Kessler, S. H., Massoli, P., Hildebrandt Ruiz, L., Fortner, E., Williams, L. R., Wilson, K. R., Surratt, J. D., Donahue, N. M., Jayne, J. T., and Worsnop, D. R.: Elemental ratio measurements of organic compounds using aerosol mass spectrometry: characterization, improved calibration, and implications, Atmos. Chem. Phys., 15, 253–272, https://doi.org/10.5194/acp-15-253-2015, 2015.
- Chen, C.-L., Chen, S., Russell, L. M., Liu, J., Price, D. J., Betha, R., Sanchez, K. J., Lee, A. K. Y., Williams, L., Collier, S. C., Zhang, Q., Kumar, A., Kleeman, M. J., Zhang, X., and Cappa, C. D.: Organic Aerosol Particle Chemical Properties Associated With Residential Burning and Fog in Wintertime San Joaquin Valley (Fresno) and With Vehicle and Firework Emissions in Summertime South Coast Air Basin (Fontana), J. Geophys. Res.-Atmos., 123, 10707–10731, https://doi.org/10.1029/2018JD028374, 2018.
- Collett, J. L., Sherman, D. E., Moore, K. F., Hannigan, M. P., and Lee, T.: Aerosol Particle Processing and Removal by Fogs: Observations in Chemically Heterogeneous Central California Radiation Fogs, Water, Air Soil Pollut. Focus, 1, 303–312, https://doi.org/10.1023/A:1013175709931, 2001.
- Collett, J. L., Herckes, P., Youngster, S., and Lee, T.: Processing of atmospheric organic matter by California radiation fogs, Atmos. Res., 87, 232–241, https://doi.org/10.1016/j.atmosres.2007.11.005, 2008.
- Collier, S., Williams, L. R., Onasch, T. B., Cappa, C. D., Zhang, X., Russell, L. M., Chen, C.-L., Sanchez, K. J., Worsnop, D. R., and Zhang, Q.: Influence of Emissions and Aqueous Processing on Particles Containing Black Carbon in a Polluted Urban Environment: Insights From a Soot Particle-Aerosol Mass Spectrometer, J. Geophys. Res.-Atmos., 123, 6648–6666, https://doi.org/10.1002/2017JD027851, 2018.
- Day, D. A., Campuzano-Jost, P., Nault, B. A., Palm, B. B., Hu, W., Guo, H., Wooldridge, P. J., Cohen, R. C., Docherty, K. S., Huffman, J. A., de Sá, S. S., Martin, S. T., and Jimenez, J. L.: A systematic re-evaluation of methods for quantification of bulk particle-phase organic nitrates using real-time aerosol mass spectrometry, Atmos. Meas. Tech., 15, 459–483, https://doi.org/10.5194/amt-15-459-2022, 2022.
- DeCarlo, P. F., Kimmel, J. R., Trimborn, A., Northway, M. J., Jayne, J. T., Aiken, A. C., Gonin, M., Fuhrer, K., Hor-

- vath, T., Docherty, K. S., Worsnop, D. R., and Jimenez, J. L.: Field-Deployable, High-Resolution, Time-of-Flight Aerosol Mass Spectrometer, Anal. Chem., 78, 8281–8289, https://doi.org/10.1021/ac061249n, 2006.
- Demoz, B. B., Collett, J. L., and Daube, B. C.: On the Caltech Active Strand Cloudwater Collectors, Atmos. Res., 41, 47–62, https://doi.org/10.1016/0169-8095(95)00044-5, 1996.
- Desyaterik, Y., Sun, Y., Shen, X., Lee, T., Wang, X., Wang, T., and Collett Jr., J. L.: Speciation of "brown" carbon in cloud water impacted by agricultural biomass burning in eastern China, J. Geophys. Res.-Atmos., 118, 7389–7399, https://doi.org/10.1002/jgrd.50561, 2013.
- Ehrenhauser, F. S., Khadapkar, K., Wang, Y., Hutchings, J. W., Delhomme, O., Kommalapati, R. R., Herckes, P., Wornat, M. J., and Valsaraj, K. T.: Processing of atmospheric polycyclic aromatic hydrocarbons by fog in an urban environment, J. Environ. Monit., 14, 2566–2579, https://doi.org/10.1039/C2EM30336A, 2012.
- Ervens, B., Carlton, A. G., Turpin, B. J., Altieri, K. E., Kreidenweis, S. M., and Feingold, G.: Secondary organic aerosol yields from cloud-processing of isoprene oxidation products, Geophys. Res. Lett., 35, https://doi.org/10.1029/2007GL031828, 2008.
- Farley, R. N., Collier, S., Cappa, C. D., Williams, L. R., Onasch, T. B., Russell, L. M., Kim, H., and Zhang, Q.: Source apportionment of soot particles and aqueous-phase processing of black carbon coatings in an urban environment, Atmos. Chem. Phys., 23, 15039–15056, https://doi.org/10.5194/acp-23-15039-2023, 2023.
- Farmer, D. K., Matsunaga, A., Docherty, K. S., Surratt, J. D., Seinfeld, J. H., Ziemann, P. J., and Jimenez, J. L.: Response of an aerosol mass spectrometer to organonitrates and organosulfates and implications for atmospheric chemistry, Proc. Natl. Acad. Sci. U. S. A., 107, 6670–6675, https://doi.org/10.1073/pnas.0912340107, 2010.
- Faust, J. A., Wong, J. P. S., Lee, A. K. Y., and Abbatt, J. P. D.: Role of Aerosol Liquid Water in Secondary Organic Aerosol Formation from Volatile Organic Compounds, Environ. Sci. Technol., 51, 1405–1413, https://doi.org/10.1021/acs.est.6b04700, 2017.
- Fierz, M., Vernooij, M. G. C., and Burtscher, H.: An improved low-flow thermodenuder, J. Aerosol Sci., 38, 1163–1168, https://doi.org/10.1016/j.jaerosci.2007.08.006, 2007.
- Ge, X., Zhang, Q., Sun, Y., Ruehl, C. R., and Setyan, A.: Effect of aqueous-phase processing on aerosol chemistry and size distributions in Fresno, California, during wintertime, Environ. Chem., 9, 221–235, 2012a.
- Ge, X., Setyan, A., Sun, Y., and Zhang, Q.: Primary and secondary organic aerosols in Fresno, California during wintertime: Results from high resolution aerosol mass spectrometry, J. Geophys. Res.-Atmos., 117, https://doi.org/10.1029/2012JD018026, 2012b.
- George, K. M., Ruthenburg, T. C., Smith, J., Yu, L., Zhang, Q., Anastasio, C., and Dillner, A. M.: FT-IR quantification of the carbonyl functional group in aqueous-phase secondary organic aerosol from phenols, Atmos. Environ., 100, 230–237, https://doi.org/10.1016/j.atmosenv.2014.11.011, 2015.
- Gilardoni, S., Massoli, P., Paglione, M., Giulianelli, L., Carbone, C., Rinaldi, M., Decesari, S., Sandrini, S., Costabile, F.,
 Gobbi, G. P., Pietrogrande, M. C., Visentin, M., Scotto, F.,
 Fuzzi, S., Facchini, M. C., Stefania, G., Paola, M., Marco, P.,
 Lara, G., Claudio, C., Matteo, R., Stefano, D., Silvia, S.,

- Francesca, C., Paolo, G. G., Chiara, P. M., Marco, V., Fabiana, S., Sandro, F., and Cristina, F. M.: Direct observation of aqueous secondary organic aerosol from biomass-burning emissions, Proc. Natl. Acad. Sci., 113, 10013–10018, https://doi.org/10.1073/pnas.1602212113, 2016.
- Haan, D. O. De, Corrigan, A. L., Smith, K. W., Stroik, D. R., Turley, J. J., Lee, F. E., Tolbert, M. A., Jimenez, J. L., Cordova, K. E., and Ferrell, G. R.: Secondary Organic Aerosol-Forming Reactions of Glyoxal with Amino Acids, Environ. Sci. Technol., 43, 2818–2824, https://doi.org/10.1021/es803534f, 2009.
- Hawkins, L. N., Lemire, A. N., Galloway, M. M., Corrigan, A. L., Turley, J. J., Espelien, B. M., and De Haan, D. O.: Maillard Chemistry in Clouds and Aqueous Aerosol As a Source of Atmospheric Humic-Like Substances, Environ. Sci. Technol., 50, 7443–7452, https://doi.org/10.1021/acs.est.6b00909, 2016.
- Hems, R. F. and Abbatt, J. P. D.: Aqueous Phase Photo-oxidation of Brown Carbon Nitrophenols: Reaction Kinetics, Mechanism, and Evolution of Light Absorption, ACS Earth Sp. Chem., 2, 225–234, https://doi.org/10.1021/acsearthspacechem.7b00123, 2018.
- Hems, R. F., Schnitzler, E. G., Bastawrous, M., Soong, R., Simpson, A. J., and Abbatt, J. P. D.: Aqueous Photoreactions of Wood Smoke Brown Carbon, ACS Earth Sp. Chem., 4, 1149–1160, https://doi.org/10.1021/acsearthspacechem.0c00117, 2020.
- Hems, R. F., Schnitzler, E. G., Liu-Kang, C., Cappa, C. D., and Abbatt, J. P. D.: Aging of Atmospheric Brown Carbon Aerosol, ACS Earth Sp. Chem., 5, 722–748, https://doi.org/10.1021/acsearthspacechem.0c00346, 2021.
- Herckes, P., Hannigan, M. P., Trenary, L., Lee, T., and Collett, J. L.: Organic compounds in radiation fogs in Davis (California), Atmos. Res., 64, 99–108, https://doi.org/10.1016/S0169-8095(02)00083-2, 2002a.
- Herckes, P., Lee, T., Trenary, L., Kang, G., Chang, H., and Collett, J. L.: Organic Matter in Central California Radiation Fogs, Environ. Sci. Technol., 36, 4777–4782, https://doi.org/10.1021/es025889t, 2002b.
- Herckes, P., Leenheer, J. A., and Collett, J. L.: Comprehensive Characterization of Atmospheric Organic Matter in Fresno, California Fog Water, Environ. Sci. Technol., 41, 393–399, https://doi.org/10.1021/es0607988, 2007.
- Herckes, P., Valsaraj, K. T., and Collett, J. L.: A review of observations of organic matter in fogs and clouds: Origin, processing and fate, Atmos. Res., 132–133, 434–449, https://doi.org/10.1016/j.atmosres.2013.06.005, 2013.
- Herckes, P., Marcotte, A. R., Wang, Y., and Collett, J. L.: Fog composition in the Central Valley of California over three decades, Atmos. Res., 151, 20–30, https://doi.org/10.1016/j.atmosres.2014.01.025, 2015.
- Herrmann, H., Schaefer, T., Tilgner, A., Styler, S. A., Weller, C., Teich, M., and Otto, T.: Tropospheric Aqueous-Phase Chemistry: Kinetics, Mechanisms, and Its Coupling to a Changing Gas Phase, Chem. Rev., 115, 4259–4334, https://doi.org/10.1021/cr500447k, 2015.
- Huang, D. D., Zhang, Q., Cheung, H. H. Y., Yu, L., Zhou, S., Anastasio, C., Smith, J. D., and Chan, C. K.: Formation and Evolution of aqSOA from Aqueous-Phase Reactions of Phenolic Carbonyls: Comparison between Ammonium Sulfate and Ammonium Nitrate Solutions, Environ. Sci. Technol., 52, 9215–9224, https://doi.org/10.1021/acs.est.8b03441, 2018.

- Jiang, W., Misovich, M. V, Hettiyadura, A. P. S., Laskin, A., McFall, A. S., Anastasio, C., and Zhang, Q.: Photosensitized Reactions of a Phenolic Carbonyl from Wood Combustion in the Aqueous Phase—Chemical Evolution and Light Absorption Properties of AqSOA, Environ. Sci. Technol., 55, 5199–5211, https://doi.org/10.1021/acs.est.0c07581, 2021.
- Jiang, W., Niedek, C., Anastasio, C., and Zhang, Q.: Photoaging of phenolic secondary organic aerosol in the aqueous phase: evolution of chemical and optical properties and effects of oxidants, Atmos. Chem. Phys., 23, 7103–7120, https://doi.org/10.5194/acp-23-7103-2023, 2023.
- Kaur, R. and Anastasio, C.: Light absorption and the photoformation of hydroxyl radical and singlet oxygen in fog waters, Atmos. Environ., 164, 387–397, https://doi.org/10.1016/j.atmosenv.2017.06.006, 2017.
- Kaur, R., Hudson, B. M., Draper, J., Tantillo, D. J., and Anastasio, C.: Aqueous reactions of organic triplet excited states with atmospheric alkenes, Atmos. Chem. Phys., 19, 5021–5032, https://doi.org/10.5194/acp-19-5021-2019, 2019.
- Kim, H., Collier, S., Ge, X., Xu, J., Sun, Y., Jiang, W., Wang, Y., Herckes, P., and Zhang, Q.: Chemical processing of water-soluble species and formation of secondary organic aerosol in fogs, Atmos. Environ., 200, 158–166, https://doi.org/10.1016/j.atmosenv.2018.11.062, 2019.
- Kuang, Y., He, Y., Xu, W., Yuan, B., Zhang, G., Ma, Z., Wu, C., Wang, C., Wang, S., Zhang, S., Tao, J., Ma, N., Su, H., Cheng, Y., Shao, M., and Sun, Y.: Photochemical Aqueous-Phase Reactions Induce Rapid Daytime Formation of Oxygenated Organic Aerosol on the North China Plain, Environ. Sci. Technol., 54, 3849–3860, https://doi.org/10.1021/acs.est.9b06836, 2020.
- Laskin, A., Laskin, J., and Nizkorodov, S. A.: Chemistry of Atmospheric Brown Carbon, Chem. Rev., 115, 4335–4382, https://doi.org/10.1021/cr5006167, 2015.
- Laskin, A., West, C. P., and Hettiyadura, A. P. S.: Molecular insights into the composition, sources, and aging of atmospheric brown carbon, Chem. Soc. Rev., 54, 1583–1612, https://doi.org/10.1039/D3CS00609C, 2025.
- Lee, A. K. Y., Hayden, K. L., Herckes, P., Leaitch, W. R., Liggio, J., Macdonald, A. M., and Abbatt, J. P. D.: Characterization of aerosol and cloud water at a mountain site during WACS 2010: secondary organic aerosol formation through oxidative cloud processing, Atmos. Chem. Phys., 12, 7103–7116, https://doi.org/10.5194/acp-12-7103-2012, 2012.
- Leresche, F., Salazar, J. R., Pfotenhauer, D. J., Hannigan, M. P., Majestic, B. J., and Rosario-Ortiz, F. L.: Photochemical Aging of Atmospheric Particulate Matter in the Aqueous Phase, Environ. Sci. Technol., 55, 13152–13163, https://doi.org/10.1021/acs.est.1c00978, 2021.
- Li, Y., Fu, T.-M., Yu, J. Z., Yu, X., Chen, Q., Miao, R., Zhou, Y., Zhang, A., Ye, J., Yang, X., Tao, S., Liu, H., and Yao, W.: Dissecting the contributions of organic nitrogen aerosols to global atmospheric nitrogen deposition and implications for ecosystems, Natl. Sci. Rev., 10, nwad244, https://doi.org/10.1093/nsr/nwad244, 2023.
- Liu, J., Gunsch, M. J., Moffett, C. E., Xu, L., El Asmar, R.,
 Zhang, Q., Watson, T. B., Allen, H. M., Crounse, J. D.,
 St. Clair, J., Kim, M., Wennberg, P. O., Weber, R. J.,
 Sheesley, R. J., and Pratt, K. A.: Hydroxymethanesulfonate
 (HMS) Formation during Summertime Fog in an Arc-

- tic Oil Field, Environ. Sci. Technol. Lett., 8, 511–518, https://doi.org/10.1021/acs.estlett.1c00357, 2021.
- Mattsson, F., Neuberger, A., Heikkinen, L., Gramlich, Y., Paglione, M., Rinaldi, M., Decesari, S., Zieger, P., Riipinen, I., and Mohr, C.: Enrichment of organic nitrogen in fog residuals observed in the Italian Po Valley, Atmos. Chem. Phys., 25, 7973–7989, https://doi.org/10.5194/acp-25-7973-2025, 2025.
- Mazzoleni, L. R., Ehrmann, B. M., Shen, X., Marshall, A. G., and Collett, J. L.: Water-Soluble Atmospheric Organic Matter in Fog: Exact Masses and Chemical Formula Identification by Ultrahigh-Resolution Fourier Transform Ion Cyclotron Resonance Mass Spectrometry, Environ. Sci. Technol., 44, 3690–3697, https://doi.org/10.1021/es903409k, 2010.
- McNeill, K. and Canonica, S.: Triplet state dissolved organic matter in aquatic photochemistry: reaction mechanisms, substrate scope, and photophysical properties, Environ. Sci. Process. Impacts, 18, 1381–1399, https://doi.org/10.1039/C6EM00408C, 2016.
- McNeill, V. F.: Aqueous Organic Chemistry in the Atmosphere: Sources and Chemical Processing of Organic Aerosols, Environ. Sci. Technol., 49, 1237–1244, https://doi.org/10.1021/es5043707, 2015.
- Ng, N. L., Canagaratna, M. R., Zhang, Q., Jimenez, J. L., Tian, J., Ulbrich, I. M., Kroll, J. H., Docherty, K. S., Chhabra, P. S., Bahreini, R., Murphy, S. M., Seinfeld, J. H., Hildebrandt, L., Donahue, N. M., DeCarlo, P. F., Lanz, V. A., Prévôt, A. S. H., Dinar, E., Rudich, Y., and Worsnop, D. R.: Organic aerosol components observed in Northern Hemispheric datasets from Aerosol Mass Spectrometry, Atmos. Chem. Phys., 10, 4625–4641, https://doi.org/10.5194/acp-10-4625-2010, 2010.
- Ng, N. L., Canagaratna, M. R., Jimenez, J. L., Chhabra, P. S., Seinfeld, J. H., and Worsnop, D. R.: Changes in organic aerosol composition with aging inferred from aerosol mass spectra, Atmos. Chem. Phys., 11, 6465–6474, https://doi.org/10.5194/acp-11-6465-2011, 2011.
- Nozière, B., Dziedzic, P., and Córdova, A.: Products and Kinetics of the Liquid-Phase Reaction of Glyoxal Catalyzed by Ammonium Ions (NH₄⁺), J. Phys. Chem. A, 113, 231–237, https://doi.org/10.1021/jp8078293, 2009.
- Ossola, R., Jönsson, O. M., Moor, K., and McNeill, K.: Singlet Oxygen Quantum Yields in Environmental Waters, Chem. Rev., 121, 4100–4146, https://doi.org/10.1021/acs.chemrev.0c00781, 2021.
- Paatero, P. and Tapper, U.: Positive matrix factorization: A non-negative factor model with optimal utilization of error estimates of data values, Environmetrics, 5, 111–126, https://doi.org/10.1002/env.3170050203, 1994.
- Pailler, L., Deguillaume, L., Lavanant, H., Schmitz, I., Hubert, M., Nicol, E., Ribeiro, M., Pichon, J.-M., Vaïtilingom, M., Dominutti, P., Burnet, F., Tulet, P., Leriche, M., and Bianco, A.: Molecular composition of clouds: a comparison between samples collected at tropical (Réunion Island, France) and mid-north (Puy de Dôme, France) latitudes, Atmos. Chem. Phys., 24, 5567–5584, https://doi.org/10.5194/acp-24-5567-2024, 2024.
- Parworth, C. L., Young, D. E., Kim, H., Zhang, X., Cappa, C. D., Collier, S., and Zhang, Q.: Wintertime water-soluble aerosol composition and particle water content in Fresno, California, J. Geophys. Res.-Atmos., 122, 3155–3170, https://doi.org/10.1002/2016JD026173, 2017.

- Pratap, V., Christiansen, A. E., Carlton, A. G., Lance, S., Casson, P., Dukett, J., Hassan, H., Schwab, J. J., and Hennigan, C. J.: Investigating the evolution of water-soluble organic carbon in evaporating cloud water, Environ. Sci. Atmos., 1, 21–30, https://doi.org/10.1039/D0EA00005A, 2021.
- Pratt, K. A., Fiddler, M. N., Shepson, P. B., Carlton, A. G., and Surratt, J. D.: Organosulfates in cloud water above the Ozarks' isoprene source region, Atmos. Environ., 77, 231–238, https://doi.org/10.1016/j.atmosenv.2013.05.011, 2013.
- Renard, P., Siekmann, F., Salque, G., Demelas, C., Coulomb, B., Vassalo, L., Ravier, S., Temime-Roussel, B., Voisin, D., and Monod, A.: Aqueous-phase oligomerization of methyl vinyl ketone through photooxidation Part 1: Aging processes of oligomers, Atmos. Chem. Phys., 15, 21–35, https://doi.org/10.5194/acp-15-21-2015, 2015.
- Roach, P. J., Laskin, J., and Laskin, A.: Higher-Order Mass Defect Analysis for Mass Spectra of Complex Organic Mixtures, Anal. Chem., 83, 4924–4929, https://doi.org/10.1021/ac200654j, 2011.
- Schneider, J., Mertes, S., van Pinxteren, D., Herrmann, H., and Borrmann, S.: Uptake of nitric acid, ammonia, and organics in orographic clouds: mass spectrometric analyses of droplet residual and interstitial aerosol particles, Atmos. Chem. Phys., 17, 1571–1593, https://doi.org/10.5194/acp-17-1571-2017, 2017.
- Schurman, M. I., Boris, A., Desyaterik, Y., and Collett Jr, J. L.: Aqueous Secondary Organic Aerosol Formation in Ambient Cloud Water Photo-Oxidations, Aerosol Air Qual. Res., 18, 15–25, https://doi.org/10.4209/aaqr.2017.01.0029, 2018.
- Shapiro, E. L., Szprengiel, J., Sareen, N., Jen, C. N., Giordano, M. R., and McNeill, V. F.: Light-absorbing secondary organic material formed by glyoxal in aqueous aerosol mimics, Atmos. Chem. Phys., 9, 2289–2300, https://doi.org/10.5194/acp-9-2289-2009, 2009.
- Smith, J. D., Kinney, H., and Anastasio, C.: Aqueous benzene-diols react with an organic triplet excited state and hydroxyl radical to form secondary organic aerosol, Phys. Chem. Chem. Phys., 17, 10227–10237, https://doi.org/10.1039/c4cp06095d, 2015.
- Sun, W., Fu, Y., Zhang, G., Yang, Y., Jiang, F., Lian, X., Jiang, B., Liao, Y., Bi, X., Chen, D., Chen, J., Wang, X., Ou, J., Peng, P., and Sheng, G.: Measurement report: Molecular characteristics of cloud water in southern China and insights into aqueousphase processes from Fourier transform ion cyclotron resonance mass spectrometry, Atmos. Chem. Phys., 21, 16631–16644, https://doi.org/10.5194/acp-21-16631-2021, 2021.
- Sun, W., Hu, X., Fu, Y., Zhang, G., Zhu, Y., Wang, X., Yan, C., Xue, L., Meng, H., Jiang, B., Liao, Y., Wang, X., Peng, P., and Bi, X.: Different Formation Pathways of Nitrogen-containing Organic Compounds in Aerosols and Fog Water in Northern China, EGUsphere [preprint], https://doi.org/10.5194/egusphere-2024-74, 2024.
- Sun, Y. L., Zhang, Q., Anastasio, C., and Sun, J.: Insights into secondary organic aerosol formed via aqueous-phase reactions of phenolic compounds based on high resolution mass spectrometry, Atmos. Chem. Phys., 10, 4809–4822, https://doi.org/10.5194/acp-10-4809-2010, 2010.
- Tomaz, S., Cui, T., Chen, Y., Sexton, K. G., Roberts, J. M.,
 Warneke, C., Yokelson, R. J., Surratt, J. D., and Turpin, B. J.:
 Photochemical Cloud Processing of Primary Wildfire Emissions as a Potential Source of Secondary Or-

- ganic Aerosol, Environ. Sci. Technol., 52, 11027–11037, https://doi.org/10.1021/acs.est.8b03293, 2018.
- Ulbrich, I. M., Canagaratna, M. R., Zhang, Q., Worsnop, D. R., and Jimenez, J. L.: Interpretation of organic components from Positive Matrix Factorization of aerosol mass spectrometric data, Atmos. Chem. Phys., 9, 2891–2918, https://doi.org/10.5194/acp-9-2891-2009, 2009.
- Wang, J., Ye, J., Zhang, Q., Zhao, J., Wu, Y., Li, J., Liu, D., Li, W., Zhang, Y., Wu, C., Xie, C., Qin, Y., Lei, Y., Huang, X., Guo, J., Liu, P., Fu, P., Li, Y., Lee, H. C., Choi, H., Zhang, J., Liao, H., Chen, M., Sun, Y., Ge, X., Martin, S. T., and Jacob, D. J.: Aqueous production of secondary organic aerosol from fossil-fuel emissions in winter Beijing haze, Proc. Natl. Acad. Sci. USA, 118, 1–6, https://doi.org/10.1073/pnas.2022179118, 2021.
- Wang, Y., Chiu, C.-A., Westerhoff, P., Valsaraj, K. T., and Herckes, P.: Characterization of atmospheric organic matter using size-exclusion chromatography with inline organic carbon detection, Atmos. Environ., 68, 326–332, https://doi.org/10.1016/j.atmosenv.2012.11.049, 2013.
- Wu, Y., Liu, Q., Liu, D., Tian, P., Xu, W., Wang, J., Hu, K., Li, S., Jiang, X., Wang, F., Huang, M., Ding, D., Yu, C., and Hu, D.: Enhanced formation of nitrogenous organic aerosols and brown carbon after aging in the planetary boundary layer, npj Clim. Atmos. Sci., 7, 179, https://doi.org/10.1038/s41612-024-00726-x, 2024.
- Youn, J.-S., Crosbie, E., Maudlin, L. C., Wang, Z., and Sorooshian, A.: Dimethylamine as a major alkyl amine species in particles and cloud water: Observations in semiarid and coastal regions, Atmos. Environ., 122, 250–258, https://doi.org/10.1016/j.atmosenv.2015.09.061, 2015.
- Young, D. E., Kim, H., Parworth, C., Zhou, S., Zhang, X., Cappa, C. D., Seco, R., Kim, S., and Zhang, Q.: Influences of emission sources and meteorology on aerosol chemistry in a polluted urban environment: results from DISCOVER-AQ California, Atmos. Chem. Phys., 16, 5427– 5451, https://doi.org/10.5194/acp-16-5427-2016, 2016.
- Yu, L., Smith, J., Laskin, A., Anastasio, C., Laskin, J., and Zhang, Q.: Chemical characterization of SOA formed from aqueous-phase reactions of phenols with the triplet excited state of carbonyl and hydroxyl radical, Atmos. Chem. Phys., 14, 13801–13816, https://doi.org/10.5194/acp-14-13801-2014, 2014.
- Yu, L., Smith, J., Laskin, A., George, K. M., Anastasio, C., Laskin, J., Dillner, A. M., and Zhang, Q.: Molecular transformations of phenolic SOA during photochemical aging in the aqueous phase: competition among oligomerization, functionalization, and fragmentation, Atmos. Chem. Phys., 16, 4511–4527, https://doi.org/10.5194/acp-16-4511-2016, 2016.
- Zhang, J., Shrivastava, M., Ma, L., Jiang, W., Anastasio, C., Zhang, Q., and Zelenyuk, A.: Modeling Novel Aqueous Particle and Cloud Chemistry Processes of Biomass Burning Phenols and Their Potential to Form Secondary Organic Aerosols, Environ. Sci. Technol., 58, 3776–3786, https://doi.org/10.1021/acs.est.3c07762, 2024.
- Zhang, Q. and Anastasio, C.: Chemistry of fog waters in California's Central Valley—Part 3: concentrations and speciation of organic and inorganic nitrogen, Atmos. Environ., 35, 5629–5643, https://doi.org/10.1016/S1352-2310(01)00337-5, 2001.

- Zhang, Q. and Anastasio, C.: Conversion of Fogwater and Aerosol Organic Nitrogen to Ammonium, Nitrate, and NOx during Exposure to Simulated Sunlight and Ozone, Environ. Sci. Technol., 37, 3522–3530, https://doi.org/10.1021/es034114x, 2003a.
- Zhang, Q. and Anastasio, C.: Free and combined amino compounds in atmospheric fine particles (PM_{2.5}) and fog waters from Northern California, Atmos. Environ., 37, 2247–2258, https://doi.org/10.1016/S1352-2310(03)00127-4, 2003b.
- Zhang, Q., Anastasio, C., and Jimenez-Cruz, M.: Water-soluble organic nitrogen in atmospheric fine particles (PM_{2.5}) from northern California, J. Geophys. Res.-Atmos., 107, AAC3-1–AAC3-9, https://doi.org/10.1029/2001JD000870, 2002.
- Zhang, Q., Jimenez, J. L., Canagaratna, M. R., Ulbrich, I. M., Ng, N. L., Worsnop, D. R., and Sun, Y.: Understanding atmospheric organic aerosols via factor analysis of aerosol mass spectrometry: a review, Anal. Bioanal. Chem., 401, 3045–3067, https://doi.org/10.1007/s00216-011-5355-y, 2011.
- Zhao, Y., Hallar, A. G., and Mazzoleni, L. R.: Atmospheric organic matter in clouds: exact masses and molecular formula identification using ultrahigh-resolution FT-ICR mass spectrometry, Atmos. Chem. Phys., 13, 12343–12362, https://doi.org/10.5194/acp-13-12343-2013, 2013.